Structure and Magnetic Properties of Oxoverdazyl Radicals and Biradicals by an Integrated Computational Approach

Vincenzo Barone,[†] Alessandro Bencini,*[,‡] Ilaria Ciofini,[§] and Claude Daul[§]

Dipartimento di Chimica, Università di Napoli "Federico II", I-80134 Napoli, Italy, Dipartimento di Chimica, Università di Firenze, 50144 Firenze, Italy, and Université de Fribourg, Institut de Chimie Inorganique et Analitique, Pérolles, 1701 Fribourg, Switzerland

Received: November 18, 1998; In Final Form: March 10, 1999

The structure, conformational behavior and magnetic properties of 1, 5-dimethyl-3-phenyl-6-oxoverdazyl radical and 1,1′,5,5′-tetramethyl-6, 6′-dioxo-3, 3′-biverdazyl biradical and of some related model compounds have been investigated by an integrated computational tool including an hybrid HF/DFT electronic method coupled to the polarizable continuum model for the description of solvent effects. The computed structural parameters are in agreement with the crystal structure for the radical and with refined post-HF computations for a simpler model compound. For the di-radical system a non planar structure is predicted both in vacuo and in solution. The nearly planar conformation found in the solid state can be ascribed to packing effect, as for the well-known biphenyl molecule. The computed exchange coupling constant of the and 1, 1′, 5, 5′ − tetramethyl-6, 6′-dioxo-3, 3′-biverdazyl di-radical is in remarkable agreement with the experimental value when averaging effects of the inter-ring torsional motion are included in the calculations.

Introduction

One of the main goals of computational chemistry is the interpretation of the conformational and spectroscopic properties of series of compounds in terms of their electronic structure, and the prediction of how these properties change when we go from an ideally isolated molecular system to the same system as it exists under experimental conditions (e.g., in solution, in the crystalline state, etc.). In the past few years the theoretical interpretation of the magnetic behavior of molecular systems has become a challenging field for the computational chemist and has led to a deeper understanding of the mechanisms of magnetic exchange.[1] In molecular magnetism, the synthesis of new molecular-based magnets is now devoted to the use of stable organic radicals as building blocks for mono- or poly-dimensional ferromagnetic materials.[2] Organic radicals have the great advantage of being easily functionalized and can also be used as bridging ligands between paramagnetic metal centers, increasing the complexity of the materials.[3] In bioinorganic chemistry, the interest toward the investigation of magnetic exchange is mostly related to the discovery of magnetostructural correlations in the active site of the metalloenzymes, and therefore to the relationships between structural deformations and magnetic properties.[4]

Ferromagnetic interactions between organic radicals are still not very common. Well-known, but few examples, of stable ferromagnetic free radicals, as galvinoxyl,[5] nitroxides,[6] nitronyl−nitroxides,[7] and binitroxides,[8] have been widely studied experimentally and theoretically characterized. The interest toward stable organic radicals that can afford ferromagnetic states upon chemical functionalization is therefore increasing. Verdazyls, whose general structure is shown in Figure 1, are known to be quite stable radicals,[9] and the peculiar magnetic properties of some of their derivatives have revived the interest of experimentalist and physicists.[10] The functionalization of the basic molecule with phenyl groups, for instance, leads to one-dimensional stacked solids that can be considered as typical examples of antiferromagnetic Heisenberg chains.[11]

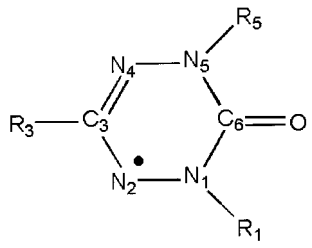

R_1=Ph, Me
R_3=Ph, Me, C(CH)$_3$, H
R_5=Ph, Me

Figure 1. General formuals of verdazyl radicals.

In the last years oxo- and thioxoverdazyl radicals[12] were synthesized and their properties investigated. In particular, the magnetic properties of 1,1′,5,5′-tetramethyl-6,6′-dioxo-3,3′-biverdazyl were studied through electron spin resonance (ESR) spectroscopy.[13] In frozen solutions of chloroform, the ground state of this system was found to be a singlet that lies 760 cm^{-1} below the next excited triplet. This biradical system also showed the peculiar feature of bridging Cu(I) ions, building up linear chains of organic radicals and metal ions, and it can be considered and studied as a building block of extended molecular magnetic systems.[14] The relatively small dimensions of the verdazyl radicals and the large amount of experimental data available on their physicochemical properties, offer the possibility to investigate their structure and conformational and magnetic behavior both in vacuo and in solution from first principles. To reliably compute physical properties, such as molecular structures and magnetic properties, of open shell

[†] Università di Napoli "Federico II".
[‡] Università di Firenze.
[§] Universitè de Fribourg.

10.1021/jp984479h CCC: $18.00
Published on Web 05/06/1999

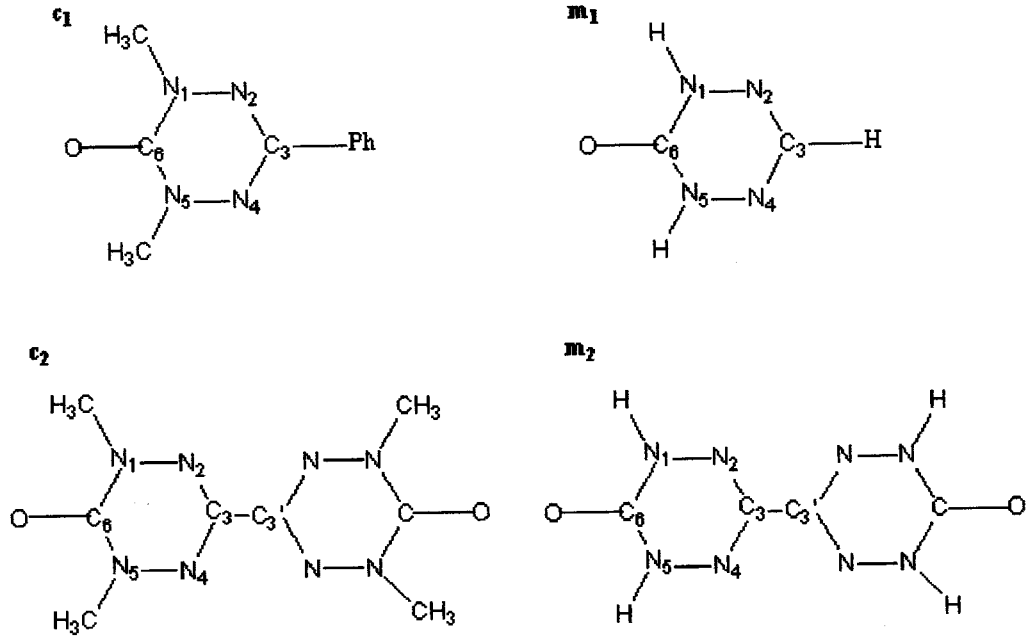

Figure 2. Structures of 1,5-dimethyl-3-phenyl-6-oxoverdazyl, **c1**, of 1,1′,5,5′−tetramethyl-6,6′-dioxo-3,3′-biverdazyl, **c2**, and of their model molecules (**m1** and **m2**).

molecules, it is necessary to take into account a significant part of the correlation energy. Despite the tremendous development of computer hardware and software, sophisticated *post*-HF methods remain often prohibitive when the complexity of the systems approaches the chemical reality or when heavy metal atoms are involved. To reduce the computational effort, density functional (DF) based methods are now widely employed.[15] The inclusion of some HF exchange in the gradient-corrected (GGA) functional seems to improve the performance of pure density functionals, especially for the calculation of molecular structures.[16] The well-known Becke three-parameter functional[17] (B3LYP) has been adopted to get reliable structures as a starting point for the calculation of different spectroscopic[18] (i.e., NMR or ESR) and magnetic properties.[19] A problem commonly encountered dealing with magnetically coupled systems is the spin contamination of low spin states by the higher spin ones. This is generally approached by the broken symmetry (BS) formalism,[20] which can be seen as an approximate spin projection and allows us to estimate the energy of a pure spin eigenstate from the energy of a single Slater determinant.

The structural, spectroscopic, and magnetic properties of oxoverdazyl radicals and biradicals are investigated in this paper by means of DF calculations based on the B3LYP functional and the BS approach. We have also analyzed the effect of the environment on the tuning of magnetic and structural characteristics of biverdazyls by applying the polarizable continuum model (PCM),[21] which afforded the interpretation[19] of the effects of the solvent on the magnetic properties of the Ullman nitroxide biradical.[22] After a short description of the systems investigated and of the computational details, the theoretical background of the calculations is exposed. Next, the computational results are analyzed and compared to the available experimental data. Finally the results obtained in the solid state and in solution are compared, and the limits of the computational approach are discussed.

Systems and the Computational Details

The general formula of oxoverdazyl derivatives is shown in Figure 1. Among all the several possible derivatives, the 1,5-dimethyl-3-phenyl-6-oxoverdazyl (**c1**) has been selected since its magnetic behavior was extensively characterized.[12a] A simpler model (**m1**), where the methyl and phenyl groups are substituted by hydrogen atoms, was also used in the calculations. The schematic structures of the molecules, **c1** (1,5-dimethyl-3-phenyl-6-oxoverdazyl) and **c2** (1,1′,5,5′-tetramethyl-6,6′-dioxo-3,3′-biverdazyl), and of their related models, **m1** and **m2**, used in the calculations are collected in Figure 2. All the calculations of **c2**, if not explicitly said, are performed on the model system **m2** where hydrogen atoms replace the four methyl groups. This model is justified by the equivalent structural and magnetic behavior computed for the optimized model **m2** and real system **c2** in vacuo (vide infra).

A modified version of Gaussian94,[23] including our recent implementation of the PCM model, was used for all the calculations. If not differently specified, the standard 6-31G* basis set was used. Density functional calculations were carried out within the unrestricted formalism using Becke's three-parameter functional,[17] which includes the Lee−Young−Parr (LYP)[24] correlation functional (B3LYP) or Becke exchange[25] and LYP correlation (BLYP).[24]

The geometrical parameters of **c1** have been computed at the UB3LYP level in vacuo. For **m2** a comparison between the molecular structures optimized on the triplet state using BLYP, ROHF, and AM1 in vacuo and B3LYP both in vacuo and in $CHCl_3$ solution was carried out. In both cases the minima were located by a full geometry optimization under the proper symmetry constraints.

Isotropic hyperfine coupling constants (hcc's) have been computed from the spin density at the corresponding nuclei using eq 1,[26] where μ_N and g_N are the nuclear magneton and

$$a(N) = \frac{8\pi}{3h} g_N g_e \mu_e \sum_{\mu,\nu} P_{\mu\nu}^{\alpha-\beta} \langle \varphi_\mu | \delta(r_k) | \varphi_\nu \rangle \qquad (1)$$

nuclear g factor, respectively, μ_e is the Bohr magneton, and g_e (electron g factor) is assumed to be equal to the g value of the free electron (2.0023), h is Plank's constant, and $P_{\mu\nu}^{\alpha-\beta}$ is the difference between the density matrices for the α and β spins.

The solvation model[21] (PCM) is a continuum model where the solute is embedded inside a cavity whose shape is defined by an interlocking sphere centered on each non-hydrogen atom. In the united atom topological model, which was used to build the cavity, the hydrogen atoms are attached to the atom they are linked to. Default values of the radii and charges, optimized for a 6-31G* basis set, were used for each hybridization of the centers. In the present calculations, values of 1.635, 1.455, 1.635, and 1.590 Å were used respectively for C, N, NH, and O. The free energy of solvation is computed as

$$\Delta G_{sol} = G_{sol} - E_{va} \tag{2}$$

where

$$G_{sol} = G_{nonelectr} + G_{es} \tag{3}$$

The nonelectrostatic terms ($G_{nonelectr} = G_{cav} + G_{disp} + G_{rep}$) are computed by classical recipes[27] and correspond to the energy necessary to build the cavity in the solvent together with the dispersion and repulsion contributions to the solute−solvent interactions. The electrostatic term (G_{es}), usually the most important for polar and charged molecules, is also the only one that enters directly into the Hamiltonian, modifying the solute electron density while the nonelectrostatic terms are just additive contributions to the total energy. A complete and exhaustive description of the model and its implementation can be found elsewhere.[28]

Theoretical Background: Magnetic Exchange Coupling Constant

To describe the magnetic interaction in coupled systems, different molecular orbital and valence bond based approaches have been used for qualitative[29] and/or quantitative descriptions. Anderson,[30] in his pioneering work, pointed out the two main contributions to the exchange coupling constant: a ferromagnetic one, which favors the parallel alignment of the spin due to the exchange interaction energy (*potential exchange*), and an antiferromagnetic one due to the overlap between the orbitals containing the unpaired electrons (*magnetic orbitals*), which favors the spin pairing (*kinetic exchange*). To get a reliable description of magnetic interactions also spin polarization effects must be included.[31] In the UHF approach spin polarization is taken into account, but the wave functions are not spin ($\mathbf{S^2}$) eigenfunctions because of the contamination of higher multiplicity spin states. This leads normally to an overestimation of the spin polarization in the UHF approach.[32] Two ways are possible to solve this problem: (i) the use of annihilation techniques and (ii) the use of the unrestricted Kohn−Sham method (UKS). In the latter case the spin polarization effects and the correlation energy are two separate contributions and there is no artificial overestimation of the spin polarization. The only problem is related to the knowledge of the exact form of the exchange and correlation functional. A complete analysis[33] of the performance of pure and hybrid (i.e., including part of the HF exchange) density functionals, recently performed on a well-known example of an exchange-coupled system, highlights that while the magnetostructural correlation trend is usually well reproduced by both models, the best agreement with the experimental structure and magnetic properties is obtained using hybrid methods such as B3LYP[17] or MPW1PW.[34]

In the present work, the broken symmetry (BS) formalism was applied to describe the multiplet structure of the system. This method, developed by Noodleman and Norman,[35] is based on a broken spin and space symmetry single determinant wave function that is able to describe the lowest spin state accounting for a large part of the electron correlation.

This BS determinant is constructed by imposing a localization of the spin on each magnetic center and a global antiparallel alignment between the two interacting centers. A relation between the energies of the BS determinant and the lowest M_s microstate of the Heisenberg−Dirac−Van Vleck, HDVV, spin Hamiltonian, $H = J\mathbf{S}_1\mathbf{S}_2$, was established. The J values can thus be calculated by considering that the energy of the BS state is a weighted average of those of the pure spin multiplets.

In the case of weakly interacting systems (overlap between the magnetic orbitals negligible) J can be computed using the formula

$$J = \frac{E(S_{max}) - E(\mathrm{BS})}{2S_1S_2} \tag{4}$$

where $E(S_{max})$ and E(BS) are the energy of the highest and broken symmetry spin states. The calculation of the energy of only two single Slater determinants suffices for the evaluation of J. A correction for the overlap between the magnetic orbitals can also be included. A rather general formalism[36] was recently applied to verify the applicability of (4) to compute the exchange coupling constant in ferromagnetic copper(II) dimers.[33] The key equation of this formalism requires the evaluation of the expectation values of $\mathbf{S^2}$. The corrected formula for two interacting spins is therefore

$$J = \frac{E(S{=}1) - E(\mathrm{BS})}{1 - b^2}$$

$$b^2 = \frac{1}{2}\langle\psi_{BS}|\mathbf{S}^2|\psi_{\mathbf{BS}}\rangle \tag{5}$$

The BS approach can also be useful in order to give a qualitative description of the exchange pathway. The BS orbitals are, in fact, usually considered as a good representation of the natural magnetic orbitals.[37]

All the following calculations are based on the BS approach, and J values are evaluated using the $\mathbf{S^2}$-corrected formula (5). The energy of triplet states were taken from spin-unrestricted single determinant calculations.

Results and Discussion

(a) 1,5-Dimethyl-3-phenyl-6-oxoverdazyl. To fully understand the electronic structure and the related properties (i.e., the hcc's) of the radical and the influence of the main geometrical parameters on them, several geometry optimizations of different computational and chemical models have been performed. All the geometry optimizations have been carried out in vacuo both for the model system **m1** and for the complete molecular system **c1**. In the case of **m1** the influence of the model chemistry on the geometry has been analyzed.

Geometry optimizations at the UB3LYP/6-31G*, UHF/6-31G*, and QCISD[38]/6-31G* levels of calculations have been performed by imposing a C_{2v} molecular symmetry. The results of the calculations are summarized in Table 1, where the bond lengths and angles computed at the various levels of approximation are compared with the X-ray structure of the analogous 1,3,5-triphenyl-6-oxoverdazyl[12a] radical. The best agreement with the experimental data is obtained by QCISD calculations, but it is worth noting that the UB3LYP/6-31G* approach gives results very close to the much more expensive post-HF

TABLE 1: Relevant Geometrical Parameters Computed in Vacuo for c1 and m1[a]

	m1[b]			**c1**[c]	**c1**[d]	
	UB3LYP/6-31G*	UHF/6-31G*	QCISD/6-31G*	UB3LYP/6-31G*	UB3LYP/6-31G*	exp[e]
$d(N_1N_2)$	1.366	1.347	1.369	1.363	1.368	1.368(1)
$d(N_2C_3)$	1.331	1.324	1.335	1.336	1.334	1.330(1)
$d(N_1C_6)$	1.387	1.366	1.382	1.389	1.390	1.381(1)
$d(C_6O)$	1.216	1.188	1.220	1.223	1.223	1.208(2)
$a(N_5C_6N_1)$	111.3	112.5	111.5	113.1	113.2	114.4
$a(C_6N_1N_2)$	126.6	125.8	126.7	124.6	125.1	124.0
$a(N_2C_3N_4)$	128.5	126.7	128.4	126.1	127.2	127.0

[a] Distances in Å; bond angles in degrees. The numbering scheme is shown in Figure 1. [b] Model system **m1**: 1,5,3-*H*-6-oxoverdazyl. [c] Real system **c1** 1,5-dimethyl-3-phenyl-6-oxoverdazyl. Coplanar rings. [d] Real system **c1** 1,5-dimethyl-3-phenyl-6-oxoverdazyl. Orthogonal rings. [e] X-ray structure of 1,3,5-triphenyl-6-oxoverdazyl from ref 12a.

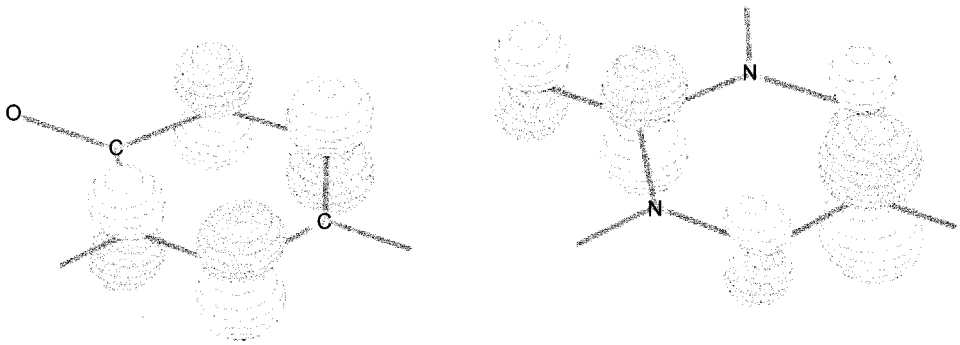

Figure 3. Isovalue representation of the SOMO (left) and LUMO (right) of **m1.** The surfaces have been drawn for $\Psi = 0.1(ea_0^{-3})^{1/2}$.

TABLE 2: Computed Isotropic Hyperfine Coupling Constants of 1,5-Dimethyl-3-phenyl-6-oxoverdazyl and Related Models[a]

	m1[b]	**m1**[c]	**c1**[d]	**c1**[e]	**c1**[f]	**m1**[b]	**m1**[b]	exp[g]
geometry	UB3LYP/6-31G*	UB3LYP/6-31G*	UB3LYP/6-31G*	UB3LYP/6-31G*	UB3LYP/6-31G*	QCISD/6-31G*	QCISD/6-31G*	
hcc's	UB3LYP/EPR-II	UB3LYP/EPR-II	UB3LYP/EPR-II	UB3LYP/EPR-II	UB3LYP/EPR-II	QCISD/EPR-II	QCISD/Chipman	
$a(2,4)N$	6.11	5.75	5.57	5.55	5.53	8.41	8.30	6.49
$a(1,5)N$	2.82	2.85	3.63	3.55	3.70	3.85	3.52	5.13

[a] Hcc's in Gauss. The numbering scheme is shown in Figure 1. [b] Model system **m1**. [c] Model system **m1** in H_2O. [d] Complex **c1** with coplanar verdazyl and phenyl rings and staggered methyl groups. [e] Complex **c1** with coplanar verdazyl and phenyl rings and eclipsed methyl groups. [f] Complex **c1** with orthogonal verdazyl and phenyl rings and staggered methyl groups. [g] ENDOR data of 1,5-dimethyl-3-phenyl-6-oxoverdazyl from ref 12a.

QCISD treatment. This demonstrates that this approach can be considered as an optimized compromise between the quality of the results and computational efforts for the determination of structural parameters. A more detailed comparison between the computed and experimental data for the model **m1** (maximum differences of 0.015 Å on bond lengths and of 0.9° on valence angles) also indicates that the influence of the methyl and phenyl substituents of the verdazyl ring on the overall geometry should be relatively small. Assuming a staggered conformation of the methyl groups (symmetry C_s), a full geometry optimization of the complete system (**c1**) has been performed using UB3LYP/6-31G*, both by imposing the coplanarity of verdazyl and phenyl ring and by their orthogonality. As shown in Table 1, no significant difference between the computed geometrical parameters and the experimental ones can be noticed, thus confirming the relatively minor influence of the substituents on the ring structure. The planar conformation has been found to be 66 kcal/mol more stable than the orthogonal one. A plausible explanation of this stabilization can be found in the efficient π-conjugation, which is effective only in the planar geometry. The symmetry of the electronic ground state is $^2A_2$ for the model, **m1**, and $^2A''$ for the real system, **c1**. In Figure 3 an isovalue representation of the SOMO and LUMO of the model **m1** is shown. The SOMO is essentially a π^* orbital with no contribution of the C and O atoms, while the LUMO is a C−O antibonding orbital with strong contribution also on the C_3 atom.

The effect of the different model chemistries on the hcc's has also been analyzed. The isotropic hcc's have been computed on the optimized structures (UB3LYP/6-31G*) of **m1** and **c1** (both in the planar and in the orthogonal conformation of the rings) using the EPR-II basis set,[39] which has been specifically tailored for the computation of ESR parameter. In Table 2, the computed hccs are compared to the experimental values.[12a] It can easily be noticed that all the computed hcc's are quite far from the experimental ones either for the model (**m1**) or for the complex (**c1**). As a matter of fact, the direct inclusion of the methyl and phenyl groups does not seem to substantially improve the computed isotropic hcc's (2.85 G vs 3.63 G) on the substituted nitrogen atoms. The effect of the rotation of the methyl groups has also been analyzed. A calculation of the hcc's for an eclipsed conformation of the methyl groups on the planar **c1** complex has also been performed. The computed isotropic hcc's are nearly the same as those computed for the staggered conformation of the methyl, as shown in Table 2.

Spin density, ρ, is a measurable quantity also via polarized neutron diffraction (PND), which has received particular attention in the past few years.[40] Although not directly related to the hcc's, which depend only on the spin density on particular nuclei, PND data have been widely used to rationalize spin coupling in organic radicals and clusters.[41] The computed spin density for **c1** is shown in Figure 4 as a surface at constant value of $\rho = 0.001ea_0^{-3}$. The unpaired spin result mainly localized on the nitrogens of the verdazyl ring. Delocalization

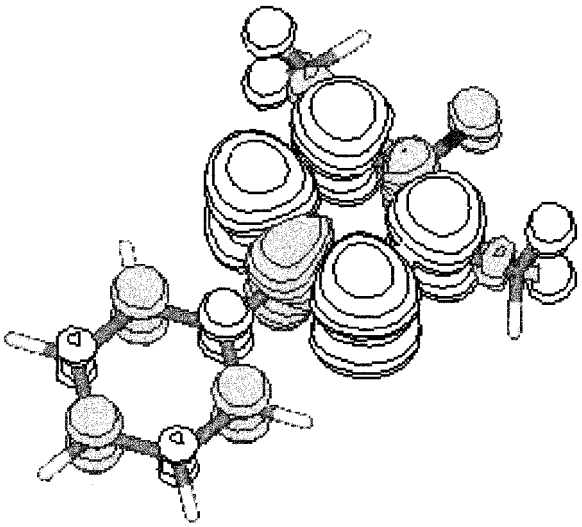

Figure 4. Isovalue representation of the spin density computed for **c1**. The surfaces have been drawn for $\rho = 0.001ea_0^{-3}$.

of the spin onto the other atoms appears to be determined mainly by spin polarization, since their spin density assumes an opposite sign with respect to the nitrogens.

The electron spin density appears to arise from two main mechanisms: direct delocalization and spin polarization. This latter mechanism, which can be called "indirect", is clearly responsible for the spin density observed on the non-nitrogen atoms, as apparent from the signs of the spin densities in Figure 4.

The effect of solvation on the computed hcc's, at the same level of modeling, for the model molecule **m1** is completely negligible, as demonstrated from the PCM UB3LYP/6-31G* calculation in H_2O (5.75 G vs 6.11 and 2.85 G vs 2.82 G). A post-HF approach was also applied in order to study more deeply the effect of electron correlation on the computed hcc's. Using the optimized QCISD/6-31G* structure of **m1,** isotropic hcc's were computed at the QCISD/EPR-II level. As reported in Table 2, the results are quite similar to the B3LYP ones, except for a larger difference between the nonequivalent nitrogen atoms. Since the EPR-II basis set was optimized for DFT methods,[39] we have repeated the QCISD computations by using the basis set optimized by Chipman (hereafter Chip) for post-HF calculations of hyperfine coupling constants in organic radicals.[42] On the one hand, it is gratifying that the results obtained by the EPR-II and Chip basis set are quite close (see Table 2). On the other hand, however, all the quantum chemical results remain quite far from the experimental values. In particular, the difference between nonequivalent nitrogen atoms obtained at the QCISD level is too large, whereas the hyperfine coupling constants computed at the DFT level are too small. Although much better results are usually obtained by this method, the relative weight of the different resonance structures is particularly difficult to estimate for open-shell systems due to the limitations of a single determinant reference model. It is then gratifying that the B3LYP method gives a fairly good ratio between the hcc's of nonequivalent nitrogens. Also the total spin densities computed at the B3LYP and QCISD levels are quite close and this is very important for a correct evaluation of the exchange coupling constant of the corresponding biradicals.

(b) 1,1′,5,5′-Tetramethyl-6,6′-dioxo-3,3′-biverdazyl Biradical. *Conformational Analysis.* As a starting point, a validation of the model used was carried out. Geometry optimizations for the model molecule, **m2**, and for the real system, **c2**, were performed in vacuo at the UB3LYP/6-31G* level for the triplet ($S = 1$) state. Relevant geometrical parameters of the computed structures are reported in Table 3 and compared with the experimental data**.** As expected, the structural parameters computed for the **c2** (full molecule) are closer to the experimental values[13] but the difference in bond lengths and angles between the model **m2** and the complex **c2** is not really significant. The main difference between computed and experimental structures is that in the X-ray structure the verdazyl rings lie in the same plane while in the computed structures they are twisted. The twisting angle is $\alpha = 34.6°$ for **m2** and $\alpha = 35.2°$ for **c2**. The planar conformation has been ascribed to packing effects (π stacking) active in the solid, and the available EPR data seem to confirm the existence of a twisted structure in solution.[13] Full geometry optimizations of the triplet state of **m2** were also carried out at the ROHF and BLYP level. The relevant geometrical parameters are shown in Table 4 where a comparison is also made with the structure obtained with the semiempirical AM1 method and the experimental values. Apart from the AM1 results, where the overestimation of the steric repulsion leads to the orthogonality of the verdazyl rings, both pure HF or DFT and mixed functional (B3LYP)[17] approaches predicted a twisted conformation with a torsion angle between 32° (BLYP) and 43° (ROHF). It can be also noticed that the inclusion of HF exchange (i.e., the passage from BLYP to B3LYP functional) determines an increase of the torsion angle and a shortening of the C_3-C_3' bond. Although all the optimized geometries are close to the experimental one, the B3LYP functional seems to better reproduce the geometrical parameters.

To fully understand the dependence of the total energy of the triplet state on the twisting angle, complete geometry

TABLE 3: Relevant Geometrical Parameters Computed in vacuo for m2 and c2 in the Triplet State and the Corresponding Exchange Coupling Constants[a]

	m2	**c2**	exp[b]
$d(C_3C_{3'})$	1.493	1.495	1.484
$d(C_3N_2)$	1.335	1.381	1.322/1.328
$d(N_1N_2)$	1.361	1.360	1.363/1.366
$d(N_1C_6)$	1.387	1.395	1.374/1.375
$d(C_6O)$	1.215	1.221	1.219
$a(N_4C_3N_2)$	127.6	127.6	128.2
$a(C_3N_2N_1)$	113.9	114.8	114.4/113.9
$a(N_2N_1C_6)$	126.8	124.9	124.4/124.9
$a(N_1C_6N_5)$	111.0	112.9	114.3
α	34.6	35.2	~0
J	566	440	760

[a] Distances in Å, bonding angles in degrees, J in cm^{-1}. The numbering scheme is shown in Figure 2. [b] From ref 13.

TABLE 4: Comparison of Relevant Geometrical Parameters Computed for m2 at Various Levels of Calculation[a]

	m2					
	AM1[v]	BLYP/ 6-31G*[c]	ROHF/ 6-31G*[b]	B3LYP/ 6-31G*[c]	B3LYP/ 6-31G*[d]	exp[b]
$d(C_3C_{3'})$	1.496	1.500	1.488	1.493	1.493	1.484
$d(C_3N_2)$	1.385	1.351	1.380	1.335	1.335	1.322/1.328
$d(N_1N_2)$	1.321	1.380	1.336	1.361	1.360	1.363/1.366
$d(N_1C_6)$	1.426	1.402	1.374	1.387	1.384	1.374/1.375
$d(C_6O)$	1.242	1.228	1.192	1.215	1.217	1.219
$a(N_4C_3N_2)$	126.7	128.2	126.1	127.6	127.4	128.2
$a(C_3N_2N_1)$	115.2	113.3	112.9	113.9	114.0	114.4/113.9
$a(N_2N_1C_6)$	123.8	127.3	126.7	126.8	126.6	124.4/124.9
$a(N_1C_6N_5)$	115.3	110.6	112.2	111.0	111.3	114.3
α	90.0	32.0	43.0	34.6	26.8	~0

[a] Distances in Å; bond angles in degrees. The numbering scheme is shown in Figure 2. [b] X-ray structure from ref 13. [c] In vacuo. [d] In $CHCl_3$.

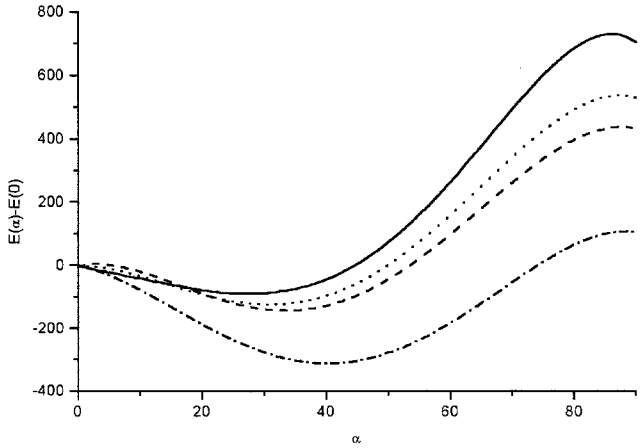

Figure 5. Potential energy profiles as a function of the torsion angle α. Triplet state energies (cm^{-1}) for (···) UBLYP, (- - -) UB3LYP, and (−·−) ROHF methods in vacuo. The solid line corresponds to PCM/UB3LYP in $CHCl_3$. The energies are scaled for the $E(0)$ of the corresponding method.

optimization, for selected torsion angles between 0° and 90°, was performed on the triplet state of **m2** within BLYP, B3LYP, and ROHF models. The potential energy profiles obtained by this approach, usually referred to as the flexible rotor model (FRM), are reported in Figure 5. All the energies of the different models were rescaled for the energy of the corresponding planar configuration ($\alpha = 0°$). Although each curve presents one single minimum, from the analysis of the potential energy profiles it is clear that the difference in energy between the conformations with $0° \leq \alpha \leq 40°$ is relatively small, especially as the HF contribution decreases. For instance, in the case of the B3LYP functional the difference in energy between the $\alpha = 0°$ and $\alpha = 40°$ conformations is only 132 cm^{-1}. A nearly free rotation in the range [0°, 40°] appears thus to be possible at room temperature in solution.

To understand the modifications induced by the solvent effects, a full geometry optimization of the triplet state was performed at the UB3LYP/6-31G* level in $CHCl_3$ (modeled with PCM).[21] The FRM approach was next used in order to get the whole potential energy profile in $CHCl_3$, which is also shown in Figure 5. As shown in Table 4, the main geometrical parameters are not greatly affected by the presence of the solvent. Only the torsional angle, α, varies significantly on passing from the vacuum ($\alpha = 35°$) to the solution ($\alpha = 27°$). Figure 5 also shows that in solution, as was already noticed in vacuo, the energy difference between the different conformers is not very large (less than 100 wavenumbers), suggesting that reliable values of the physicochemical properties of biverdazyls can be obtained only after proper averaging over the torsional motion (vide infra). An increase of the relative stability of planar or nearly planar structures in solution is also observed, probably due to an easier polarization of the π-electrons by the solvent. Note that biverdazyl has a vanishing dipole moment irrespective of the particular conformation adopted. As a consequence, the simple Onsager model (dipole in a sphere) would predict a constant solvation energy.

The preference for a twisted conformation in the triplet state is probably related to the competition between electronic and steric factors. From a steric point of view, the orthogonal conformation is obviously preferred, while from an electronic point of view inter-ring electron delocalization is maximized in planar or nearly planar structures. An isodensity representation of the highest SOMO and of the LUMO of the triplet state of **m2** is given in Figure 6. The more stable SOMO essentially results from an antibonding interaction between the π^* orbital centered on each ring, whereas the LUMO shows an extensive delocalization through the C_3-C_3' atoms. This orbital plays the dominant role in the zwitterionic diamagnetic form of the system.

Magnetostructural Correlation. The magnetic behavior of the bi-verdayl radical has been studied by computing the energy of the BS state on each of the FRM triplet geometries of **m2**. From these calculations the exchange coupling constants, J (i.e. the singlet−triplet splitting), were computed by applying the overlap correct formula (5). The spin contamination on the BS wave function was always quite small ($S^2 \ll 1$) and therefore the correction applied was usually very small. Therefore, for weakly interacting systems, the two formulas (4) and (5) lead to very close results. The computed J values are shown in Figure 7 and compared to the experimental figures as measured in a solid (887 cm^{-1}) and in solution (760 cm^{-1}).[13] The two slightly different values for the solid state and the solution suggest that a different conformation of the biradical is present in the two states of aggregation. The higher values in the solid state (planar configuration) are also consistent with the computed values of J for $\alpha \rightarrow 0°$.

Since the difference in energy between the different conformations near the minimum geometry is rather small, we have computed average values of J, $\langle J \rangle$, over the inter-ring torsional motion, by following a procedure described in detail in previous works.[43] The computed $\langle J \rangle$ values are collected in Table 5. The values calculated in vacuo and in solution, 721 and 844 cm^{-1} at 298 K, respectively, are rather close together, and the increase with the polarity of the solvent is in better agreement with the larger value measured in the solid state than with that in the frozen solution. As a matter of fact this results from an indirect

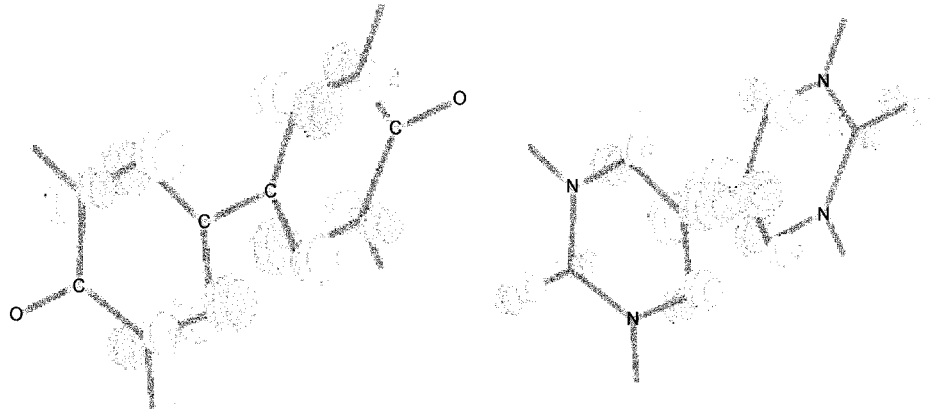

Figure 6. Isovalue representation of the SOMO (left) and LUMO (right) of **m2.** The surfaces have been drawn for $\Psi = 0.1(ea_0^{-3})^{1/2}$.

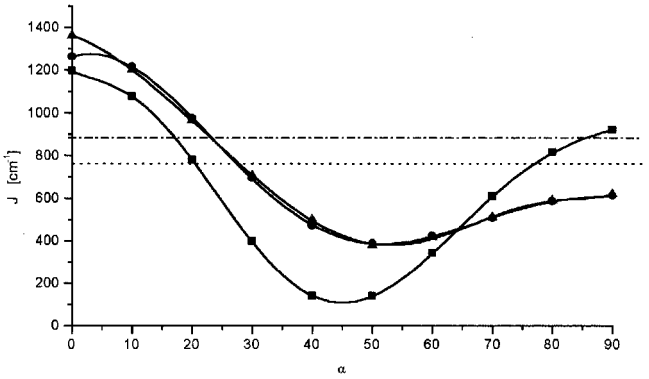

Figure 7. Computed dependence of J for **m2** on the torsion angle, α (see text): PCM/UB3LYP (●); UBLYP/vacuo (■); UB3LYP/vacuo (▲). Experimental values in frozen chloroform solution (···) and in solid state (−·−) are also plotted.

TABLE 5: Averaged J Values (cm^{-1}) over the Inter-ring Torsional Motion (α) in Vacuo and $CHCl_3$ Solution for m2

	in vacuo[a]	$CHCl_3$
α_{min}, deg	34.6	26.8
J_{min}	566.1 (606.3)	757.0
$\langle J \rangle$ (0 K)	585.2 (601.1)	774.4
$\langle J \rangle$ (298 K)	721.2 (729.6)	844.3

[a] The values in parentheses have been obtained using the geometries computed in vacuo and J computed in $CHCl_3$.

solvent effect, namely, the reduction of the average out of plane angle previously discussed. The values enclosed in parentheses in Table 5 have been computed using the geometries obtained in vacuo and include the solvent effects the energies of the triplet and the BS state are calculated. This direct solvent effect (i.e., modification of $\langle J \rangle$ at a constant geometry) is much smaller than the indirect one, i.e. the effect of the geometrical variations induced by the solvent. A marked dependence of $\langle J \rangle$ on the temperature is also computed, which reflects the fact that more conformations become populated at higher temperatures, since the potential surface near the minimum is flat and therefore the corresponding vibrational states are very close in energy and delocalized.

FRM calculations have been performed also for the BS state, both in vacuo and in $CHCl_3$. The computed energy as a function of the α angle is reported in Figure 8 and compared to the energy of the triplet state. The minimum energy conformation for the BS state corresponds to a planar configuration, while the maximum is consistent with the orthogonality of the rings. Since the J values reported in Figure 7 are proportional to the triplet−BS energy gap through eq 5, they are not linearly dependent on the α angle. In Figure 9 a picture of the magnetic orbital containing the α electron, as obtained by the BS calculation, is shown. The orbital is localized onto the one of the two verdazyl rings, the degenerate orbital corresponding to the β electron being localized onto the other ring. According to qualitative considerations,[37] it can be noticed that the antiferromagnetic contribution to J decreases with the overlap between the magnetic orbitals and therefore is consistent with a stabilization of the planar conformation (maximum overlap) for the antiferromagnetic spin-coupled state. This is reflected by the dependence of the energy of the BS state on the torsion angle α. On the contrary, as previously explained, for the triplet state we notice that a twisted form is more stable (even if the differences in energy are small). Therefore, while being always antiferromagnetic, the global dependence of J on α is not linear.

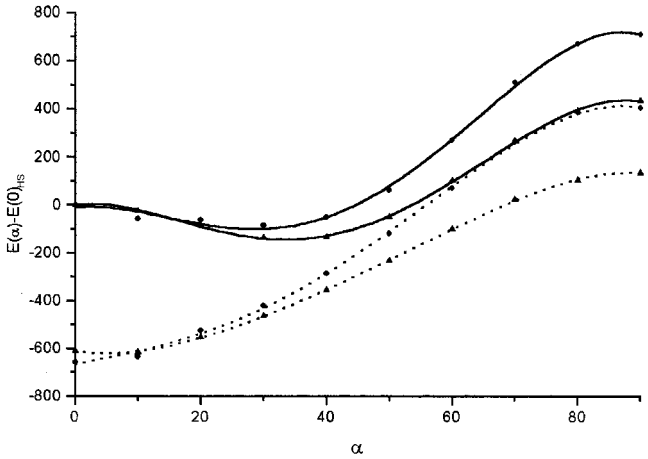

Figure 8. Potential energy profiles as a function of the torsion angle α computed for **m2** on the triplet and broken symmetry (BS) states using UBLYP76-31G* in vacuo and in $CHCl_3$. Triplet (−·−) and BS (··●··) states in vacuo and triplet (−▲−) and BS (··▲··) states in $CHCl_3$. All the energies (cm^{-1}) are scaled for the E(0) of the corresponding triplet state.

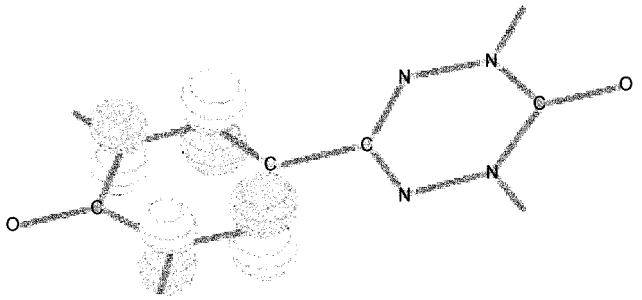

Figure 9. Isovalue representation of the α magnetic orbital of **m2** (see text) The surfaces have been drawn for $\Psi = 0.1(ea_0^{-3})^{1/2}$.

Conclusion

A powerful HF/DF hybrid (the B3LYP model) has been used to investigate the structural, conformational, and magnetic properties of the oxoverdazyl radical and of the biradical obtained by joining two identical units. Moreover, solvent effects have been taken into account by a refined continuum solvent model (PCM) and vibrational averaging over large amplitude motions has also been taken into account.

Comparison with experimental data and with refined post-HF computations for simplified model compounds confirm the reliability of our approach and provide further insight into the role played by intrinsic and environmental effects in determining the physicochemical properties of organic biradicals.

Although direct solvent effects have been found to have negligible effects on the magnitude of the magnetic coupling, they severely influence the torsional potential for rotation around the inter-ring bond, which, in turn, brings the vibrationally averaged values of J in closer agreement with the experimental data.

The hcc's computed on the nitrogen atoms are remarkably different from the experimental values and are the only observables that could not be satisfactorily reproduced. Both geometrical and environmental effects do not significantly affect the computed values, which are in any case rather far from experiment. The ratio between the hcc's is also different from that experimentally found, i.e., 2.0:2.3 for $\mathbf{m_1}$ and 1.5:1.6 for $\mathbf{c_1}$, vs 1.3. This fact can probably indicate that a multireference CI approach is needed in the present case. For such a large

molecular system, the computer cost of this approach is prohibitive and has not been attempted.

From a more general point of view, the present study contributes to paving the route for the investigation of a large magnetic system in condensed phases. This becomes increasingly more valid since the whole computational protocol is or will be shortly available to other researchers in the field through standard quantum chemical packages.

Acknowledgment. This work was supported by the Swiss National Foundation and the COST Action D9.

References and Notes

(1) (a) Miralles, J.; Daudey, J.-P.; Caballol, R. *Chem. Phys. Lett.* **1992**, *198*, 555. (b) Castell, O.; Miralles, J. Caballol, R. *J. Chem. Phys.* **1994**, *179*, 377. (c) Caballol, R.; Castell, O.; Illas, F.; Moreira, I. de P. R.; Malrieu. *J. Phys. Chem. A* **1997**, *101*, 7860. (d) Cuelemans, A.; Heylen, G. A.; Chibotaru, L. F.; Maes, T. L.; Pierloot, K.; Ribbing, C.; Vanquickenborne, L. G. *Inorg. Chim. Acta* **1996**, *251*, 15. (e) *Molecule-Based Magnetic Materials: Theory, Techniques, and Applications*; Turnbull, M. M., Sugimoto, T., Thompson, L. K., Eds.; ACS Symposium Series 644; Washington, DC, 1966.

(2) (a) Awaga, K.; Sugano, T.; Kinoshita, M. *Solid State Commun.* **1986**, *57*, 453. *(*b) Awaga, K.; Maruyama, Y. *J. Chem. Phys.* **1989**, *91*, 2743. (c) Veciana, J.; Rovira, C.; Armet, O.; Domingo, V. M.; Crespo, M. I.; Palacio, F. *J. Am. Chem. Soc.* **1991**, *113*, 2552. (d) Rajca, A. Utamapayana, S. *J. Am. Chem. Soc.* **1993**, *115*, 2396.

(3) (a) Benelli, C.; Caneschi, A.; Gatteschi, D.; Pardi, L. In *Magnetic Molecular Material*; Gatteschi, D., Kahn, O., Miller, J. S., Palacio, F., Eds.; Kluwer: Dordrecht, The Netherlands, 1991; p 233. (b) Caneschi, A.; Gatteschi, D.; Rey, P. *Prog. Inorg. Chem.* **1991**, *39*, 331. (c) Dei, A.; Gatteschi, D. *Inorg. Chim. Acta* **1992**, 813.

(4) (a) Sauer, K. *Acc. Chem. Res.* **1980**, *13*, 249. (b) *Iron*−*Sulfur Proteins*; Spiro, T. G., Ed.; Wiley and Sons: new York, 1982. (c) *Iron*−*Sulfur Proteins*; Cammack, R., Ed.; Advances in Inorganic Chemistry, Vol. 38; Academic Press: San Diego, 1992. (d) Barber, J. *Nature* **1995,** *376*, 388. (e) Holm, R. H.; Kennepohl, P.; Solomon, E. I. *Chem. Rev.* **1996**, *96*, 2239.

(5) (a) Mukai, K. *Bull. Chem. Soc. Jpn.* **1969**, *42*, 40. (b) Kinoshita, M. *Mol. Cryst. Liq. Cryst.* **1989**, *176*, 163.

(6) Nogami, T.; Tomioka, K.; Ishida, T.; Yoshikawa, H.; Yasui, M.; Iwasaki, F.; Iwamura, H.; Takeda, N.; Ishikawa, M. *Chem. Lett.* **1994**, 29.

(7) (a) Awaga, K.; Inabe, T.; Nakamura, T.; Matsumoto, M.; Maruyama, Y. *Mol. Cryst. Liq. Cryst. A* **1993**, *232*, 69. (b) Awaga, K.; Inabe, T.; Nakamura, T.; Matsumoto, M.; Maruyama, Y. *Synth. Met.* **1993**, *56*, 3311.

(8) Chiarelli, R.; Novak, M. A.; Rassat, A.; Tholence, J. L. *Nature* **1993**, *363*, 147

(9) (a) Kuhn, R.; Trischmann, H. *Angew. Chem.* **1963**, *75*, 294. (b) Kuhn, R.; Trischmann, H. *Monatsh. Chem.* **1964**, *95*, 457.

(10) (a) Azuma, N.; Yamauchi, J.; Mukai, K.; Ohya-Nishiguchi, H.; Deguchi, Y. *Bull. Chem. Soc. Jpn.* **1973**, *46*, 2728. (b) Takeda, K.; Deguchi, H.; Hoshiko, T.; Konishi, K.; Takahashi, K.; Yamauchi, J. *J. Phys. Soc. Jpn.* **1989**, *58*, 3361.

(11) (a) Dormann, E.; Winter, H.; Dyakonow, W.; Gotschy, B.; Lang, A.; Naarmann. H.; Walker, N. *Ber. Bunsen-Ges. Phys. Chem.* **1992**, *96*, 922. (b) Lang, A.; Naarmann, H.; Walker, N.; Dormann, E. *Synth. Met.* **1993**, 53, 379. (c) Dormann, E.; Dyakonow, W.; Gotschy, B.; Lang, A.; Naarmann, H.; Pilawa, B.; Walker, N. *Ber. Bunsen-Ges. Phys. Chem.* **1993**, *55*, 5−57, 3273. (d) Pilawa, B.; Pietrus, T. *J. Magn. Mater.* **1995**, 150, 165.

(12) (a) Neugerbauer, F. A.; Fisher, H.; Krieger, C. *J. Chem. Soc., Perkin Trans. 2* **1993**, 535. (b) Kremer, R. K.; Kanellakopulos, B.; Bele, P.; Brunner, H.; Neugerbauer, F. A. *Chem. Phys. Lett.* **1994**, *230*, 255. (c) Ballüder, K.; Kelemen, M.; Pérez, F.; Pilawa, B.; Watcher, C.; Dormann, E. *Ber. Bunsen-Ges. Phys. Chem.* **1997**, *101*, 1882. (d) Mukai, K.; Nuwa, M.; Suzuki, K.; Nagaoka, S.; Achiwa, N.; Jamali, J. B. *J. Phys. Chem. B* **1998**, *102*, 782.

(13) Brook, D. J.; Fox, H. H.; Lynch, V.; Fox, M. A. *J. Phys. Chem.* **1996**, *100*, 2066.

(14) Brook, D. J.; Lynch, V.; Conklin, B.; Fox, M. A. *J. Am. Chem. Soc.* **1997**, *119*, 5155.

(15) Barone, V. In *Recent Advances in Density Functional Methods, Part I*; Chong, D. E., Ed.; World Scientific: Singapore, 1995; p 287.

(16) (a) Adamo, C.; Barone, V.; Fortunelli, A. *J. Chem. Phys.* **1995**, *102*, 384. (b) Barone, V. *Theor. Chim. Acta* **1995**, *91*, 113.

(17) Becke, A. D. *J. Chem. Phys.* **1993**, *98*, 5648.

(18) (a) Cheesman, J. R.; Trucks, G. W.; Keith, T. A.; Frish, M. J. *J. Chem. Phys.* **1996**, *104*, 5497. (b) O'Malley, P. J. *Chem. Phys. Lett.* **1998**, *285*, 99.

(19) Barone, V.; Bencini, A.; di Matteo, A. *J. Am. Chem. Soc.* **1997**, *119*, 10831.

(20) (a) Noodlemann, L.; Davidson, E. R. *Chem. Phys.* **1979**, *70*, 4903. (b) Noodlemann, L. *J. Chem. Phys.* **1981**, *74*, 5737.

(21) (a) Cossi, M.; Barone, V.; Cammi, R.; Tomasi, *J. Chem. Phys. Lett.* **1996**, *235*, 327. (b) Barone, V.; Cossi, M.; Rega, N. *J. Chem. Phys.* **1996**, *105*, 11060.

(22) Ullman, E. F.; Boocock, D. G. B. *J. Chem. Soc., Chem. Commun.* **1961**, 1161.

(23) Frish, M. J.; Trucks, G. W.; Schlegel, H. B.; Gill, P. M. W.; Johnson. B. G.; Robb, M. A.; Cheeseman, J. R.; Keith, T. A.; Petersson, G. A.; Montgomery, J. A.; Rsghavachari, K.; Al-Laham, M. A.; Zakrewski, V. G.; Ortiz, J. V.; Foresman, J. B.; Cioslowski, J.; Stefanov, B. B.; Nanayakkara, A.; Challacombe, M.; Peng, C. Y.; Ayala, P. Y.; Chen, W.; Wong, M. W.; Andres, J. L.; Replogle, E. S.; Gomperts, R.; Martin, R. L.; Fox, D. J.; Binkley, J. S.; DeFrees, D. J.; Baker, J.; Stewart, J. P.; Head-Gordon, M.; Gonzales, C.; Pople, J. A. *Gaussian 94*; Gaussian Inc.: Pittsburgh, PA, 1996.

(24) Lee, C.; Yang, W.; Parr, R. G. *Phys. Rev. B* **1988**, *37*, 785.

(25) Becke, A. D. *Phys. Rev A* **1988**, *38*, 3098.

(26) Weltner, W. *Magnetic Atoms and Molecules*; Van Nostrand: New York; 1983.

(27) (a) Cammi, R.; Tomasi, J. *J. Chem. Phys.* **1994**, *101*, 3888. (b) Cossi, M.; Tomasi, J.; Cammi, R. *Int. J. Quantum Chem. Quantum Chem. Symp.* **1995**, *29*, 625.

(28) Amovilli, C.; Barone, V.; Cammi, R.; Camces, E.; Cossi, M.; Mennucci, B.; Pomelli, C. S.; Tomasi, J. *Adv. Quantum Chem.* **1998**, 31.

(29) (a) Goodenough, J. B. *Phys. Rev.* **1955**, *100*, 564. (b) Goodenough, J. B. *Phys. Chem. Solids* **1958**, *6*, 287. (c) Kanamori, J. *Phys. Chem. Solids* **1959**, *10*, 87.

(30) (a) Anderson, P. W. In *Magnetism*; Rado, G. E., Ed.; Academic Press: New York, 1963; Vol. I. (b) Anderson, P. W.; Hasegawa, H. *Phys. Rev.* **1968**, *100*, 675.

(31) McConnel, H. M. *Chem. Phys.* **1963**, *36*, 1910.

(32) Chipman, D. M. *Theor. Chim. Acta* **1992**, *82*, 93.

(33) Adamo, C.; Barone, V.; Bencini, A.; Ciofini, I.; Totti, F. *Inorg. Chem.*, in press.

(34) Adamo, C.; Barone, V. *J. Chem. Phys.* **1998**, *108*, 664.

(35) (a) Noodleman, L.; Case, D. A. *Adv. Inorg. Chem.* **1992**, *38*, 423. (b) Noodleman, L.; Norman, J. G. *J. Chem. Phys.* **1979**, *79*, 4903.

(36) Ovchinnikov, A. A.; Labanowski, J. K. *Phys. Rev. A* **1996**, *53*, 3946.

(37) Kahn, O. In *Molecular Magnetism*; VCH: New York, 1993.

(38) Pople, A. J.; Head-Gordon, M.; Raghavachari, K. *J. Chem. Phys.* **1987**, *87*, 5968.

(39) Barone, V. *J. Chem. Phys.* **1994**, *101*, 6834.

(40) Gillon, B.; Schweizer, J. In *Molecules in Physics, Chemistry, and Biology*; Maruani, J., Ed.; Kluwer Academic Publisher: Dordrecht, The Netherlands, 1989; Vol. III, p 111.

(41) (a) Zheludev, A.; Bonnet, M.; Ressouche, E.; Schweizer, J.; Wan, M.; Wang, H. *J. Magn. Magn. Mater.* **1994**, *135*, 147. (b) Caneschi, A.; Gatteschi, D.; Sessoli, R.; Schweizer, J. *Physica* **1998**, *B241*−*243*, 600.

(42) Chipman, D. M. *Theor. Chim. Acta* **1992**, *82*, 93.

(43) (a) Barone, V.; Minichino, C. *THEOCHEM* **1995**, *330*, 365. (b) Barone, V. *J. Phys. Chem.* **1995**, *99*, 11659.